



## Distribution and time-variation of spire streaks at Pavonis Mons on Mars

T. Toyota<sup>a,b,\*</sup>, K. Kurita<sup>b</sup>, A. Spiga<sup>c,d</sup>

<sup>a</sup> Department of Earth and Planetary Science, The University of Tokyo, Tokyo, Japan

<sup>b</sup> Earthquake Research Institute, The University of Tokyo, Tokyo, Japan

<sup>c</sup> Laboratoire de Météorologie Dynamique, Université Pierre et Marie Curie, Paris, France

<sup>d</sup> Department of Physics and Astronomy, The Open University, Milton Keynes, United Kingdom

### ARTICLE INFO

#### Article history:

Received 8 June 2010

Received in revised form

25 January 2011

Accepted 25 January 2011

Available online 21 February 2011

#### Keywords:

Mars

Wind streak

Tharsis volcano

Pavonis Mons

### ABSTRACT

We documented the distribution and the time-variation of the specific dark wind streaks at Pavonis Mons. We focused on the streaks we named “Spire Streaks”, which are overlapping spindle shaped dark streaks at the upper boundary of the coalesced dark streaks on Tharsis volcanoes. We investigated both visible and infrared images obtained by Viking orbiter camera, Mars Orbiter Camera (MOC), THEMIS, CTX and HiRISE of the spire streaks at Pavonis Mons. We also used topographic data obtained by Mars Orbiter Laser Altimeter (MOLA) to see the relationship between the topography and the distribution of the spire streaks. The spire streaks at Pavonis Mons provide us high-resolution information about the direction of the nighttime slope wind, and could be indirect clues for the time-variation of the nighttime environment. We conclude that the spire streaks are erosional features. However, some features of the spire streaks reported in this paper are outside the scope of previous modeling for erosional process, and we need a new category of model for the formation.

© 2011 Elsevier Ltd. All rights reserved.

### 1. Introduction

On the planets with atmospheres such as Mars, there are various types of interactions between the atmosphere and the ground surface. Such interactions cause observable changes on the surface in the form of tonal (albedo) or textural patterns, with which we can trace the activities of atmosphere (Geissler, 2005). Coalesced dark streaks encircling the summit of the Martian Montes are examples of these (Figs. 1(A) and 2).

Coalesced dark streaks at the upper slopes of Tharsis volcanoes were first discovered in Mariner 9 photography (Sagan et al., 1974). Since fine-grained dust appears brighter than coarse-grained materials (Singer and Roush, 1983; Wells et al., 1984; Fischer and Pieters, 1993), they suggested that the dark feature was due to removal of surface cover of fine-grained particles. Following research took their idea further, and suggested the summit-encircling morphology is formed by daily activity of nighttime slope wind (Thomas et al., 1981, 1984; Lee et al., 1982; Greeley et al., 2003).

Coalesced dark streaks, which are named by Thomas et al. (1981) and Lee et al. (1982), are large (from several ten to hundred kilometers) dark markings without recognizable

topographic obstacles at the origin. The boundaries of these markings are serrate with the coalesced streaks. The concept of removal of fine-grained particles appears to be plausible (Thomas et al., 1981; Lee et al., 1982), and basic modeling of formation of the coalesced dark streaks has already been presented (Magalhaes and Gierasch, 1982).

Recent high-resolution observations have revealed several features of the coalesced dark streaks, which could not be observed in the past. The High Resolution Imaging Science Experiment (HiRISE) onboard Mars Reconnaissance Orbiter revealed tens of centimeter-scaled surface features of the coalesced dark streaks (e.g. reticulate textures, Bridges et al., 2010). Such small-scaled features are worth investigating to make sure whether the coalesced dark streaks are consistent with the previous modeling for the formation.

Here we focus on the streaks we named spire streaks at Pavonis Mons. The spire streaks are overlapping spindle shaped dark streaks at the upper boundary of the coalesced dark streaks (see Fig. 1(B) right and Fig. 4). Spire streaks are part of coalesced dark streaks. They have relatively clear rectilinear boundaries and smaller sizes among the coalesced dark streaks. Slope streaks, which are common dark features prevalent throughout dust-rich equatorial regions of Mars, are also examples of spindle shaped dark streaks (Sullivan et al., 2001; Chuang et al., 2007, 2010). However, (1) the spire streaks have much larger scale than the slope streaks, (2) there is no sharp boundary of the physical texture of the surface between inside and outside the spire streaks, although many of the slope streaks

\* Corresponding author at: Earthquake Research Institute, The University of Tokyo, 1-1-1 Yayoi, Bunkyo-Ku, Tokyo 113-0032, Japan. Tel.: +81 3 5841 5728.  
E-mail address: [toyota@eri.u-tokyo.ac.jp](mailto:toyota@eri.u-tokyo.ac.jp) (T. Toyota).

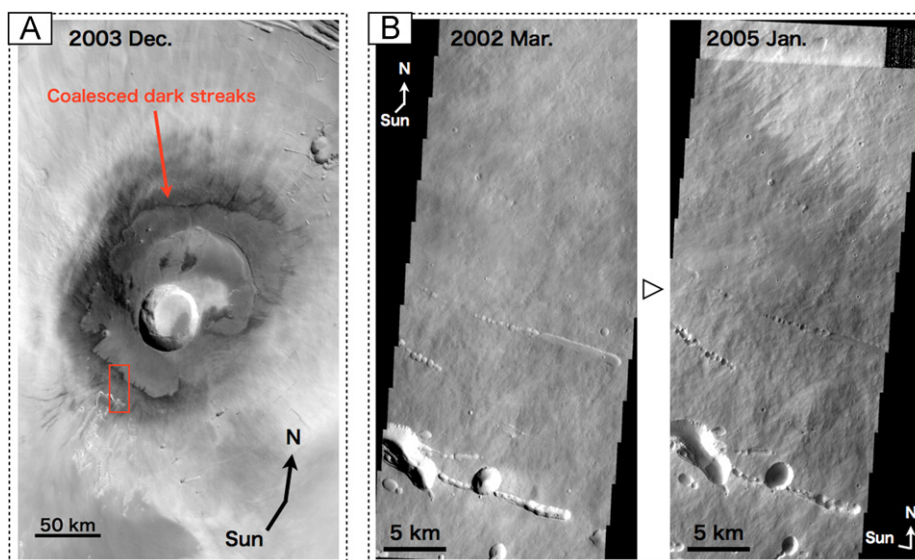


**Fig. 1.** (A) Image of Pavonis Mons (ref. no. R12-03502) taken by Mars Orbiter Camera (MOC) onboard Mars Global Surveyor (MGS). This image is not map projected. The dark albedo feature, called “coalesced dark streaks”, can be seen on the flanks of Pavonis Mons in the Tharsis region. (B) Temporal changes of the coalesced dark streaks at the red square in (A) from 2002 to 2005. Both images were taken by THEMIS VIS. The spire streaks which are not seen in the left image (V01302016, 2002/03/31,  $L_s=350.92^\circ$  incidence angle  $=48.33^\circ$ , phase angle  $=48.36^\circ$ ) appeared in the right image (V13610001, 2005/01/07,  $L_s=140.89^\circ$ , incidence angle  $=82.54^\circ$ , phase angle  $=82.55^\circ$ ). These images are close-ups of the variation which is also seen in Fig. 8(B). The seasonal and annual variations of the globally averaged dust optical depth between the two images seem to be smaller than 0.1 (Smith, 2004, 2009). This temporal change of the streaks was observed by not only THEMIS but also MGS MOC. (For interpretation of the references to color in this figure legend, the reader is referred to the web version of this article.)

have, (3) the spire streaks are usually observed at where the inclination of the slope changes (not at the halfway down the slope), (4) the spire streaks are observed at the upper boundary of the coalesced dark streaks. We rarely observe that a spindle shaped spire streak alone without the large dark albedo feature at the lower side of the spire streak.

In this paper, we report the specific characteristics of the spire streaks at Pavonis Mons because of dense image coverage although they are commonly observed at other Tharsis volcanoes (Fig. 2). We investigated the morphology, the distribution and the time-variation of the spire streaks on Pavonis Mons. Combining these observations with a numerical simulation for the slope wind, we propose that the spire streaks provide information on nighttime slope wind at the volcanoes and some features of the spire streaks are not previously modeled.

## 2. Method

### 2.1. Observations

We investigated both visible and infrared images obtained by Viking orbiter camera (Carr et al., 1972), Mars Orbiter Camera (MOC) (Malin et al., 1992), THEMIS (Christensen et al., 2004), CTX (Malin et al., 2007) and HiRISE (McEwen et al., 2007) of the spire streaks at Pavonis Mons. We also used topographic data obtained by Mars Orbiter Laser Altimeter (MOLA) (Zuber et al., 1992) to see the relationship between the topography and the distribution of the spire streaks. We used the MOLA Mission Experiment Gridded Data Records (MEGDRs) which have the resolution of 128 pixels per degree. Tables 1 and 2 respectively show the list of instruments and images we investigated.

### 2.2. Modeling

Maps of near-surface winds would be useful to understand the possible erosional origin of spire streaks, however measurements of wind are unfortunately not available in the Tharsis region we

chose to focus on. Instead we rely on predictions from physically consistent mesoscale atmospheric modeling. Information on near-surface winds relevant for the lifting has been gained from general circulation modeling (e.g. Newman et al., 2002), however mesoscale models allow for resolving the atmospheric flow (and notably the impact of topography on it) at finer scales than general circulation models (e.g. Spiga and Lewis, 2010). In this paper we employ the high-resolution mesoscale model described in Spiga and Forget (2009), which calculates the evolution of the atmospheric flow under constraints imposed by radiative forcings by atmospheric  $\text{CO}_2$  and airborne dust, soil diffusion and boundary layer mixing. Further details about model settings, typical simulations and comparisons with available measurements and independent simulations are described in Spiga and Forget (2009). We use a specific simulation for the Pavonis Mons case at northern fall equinox with a grid spacing of 6 km (enough to resolve accurately the slopes of the volcano) on a limited-area domain 600 km across, centered on the volcano.

To discuss whether material is able to be lifted and saltated (or suspended) over the surface by atmospheric winds, a key parameter is friction velocity  $u_*$ . It is related to near-surface wind stress  $\tau$  through the relationship  $\tau = \rho u_*^2$ . In atmospheric levels close to the surface, wind speed varies approximately logarithmically with height  $ku(z) = u_* \ln z / z_0$  where  $k=0.4$  is the von Karman constant and  $z_0$  the roughness length (a value of 1 cm for  $z_0$ , thought to be typical for Martian conditions, is adopted in this study similarly to most studies in the literature, e.g. Newman et al., 2002). Hence  $u_*$  can be deduced through the relationship  $u_* = ku(z_1) / \ln z_1 / z_0$  from near-surface winds  $u(z_1)$  simulated by the Spiga and Forget (2009) mesoscale model in the first vertical level above the surface, at an altitude of about  $z_1=3$  m. This is the method used to obtain Figs. 9 and 10 discussed in Section 5.

## 3. Description of spire streaks at Pavonis Mons

Coalesced dark streaks are observed near the summit area of high mountains such as the Tharsis Montes (Figs. 1(A) and 2). The

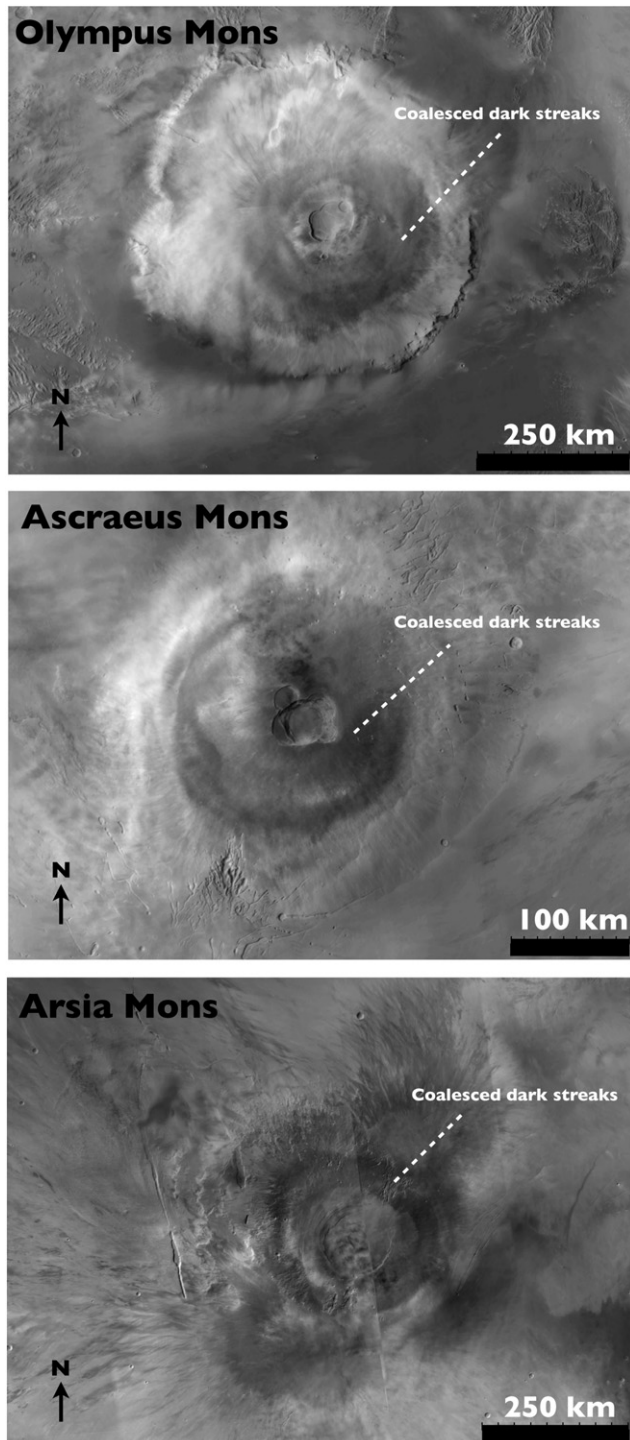


**Fig. 2.** Coalesced dark streaks (relatively dark surfaces indicated by white dashed lines) at Olympus, Arsia and Ascræus Mons. Coalesced dark streaks are observed near the summit area of the volcanoes. These images are mosaics assembled from wide angle red images (primarily those acquired in May–June 1999) from the Mars Orbiter Camera (see <http://www.msss.com/mgcvw/mgm/> for additional information).

common feature in the distribution of coalesced dark streak is its highest position; the inner most position of the dark feature. In most cases, volcanoes with the coalesced dark streaks have a caldera and the surface slope around the caldera are gentle while the lower flanks are steeper. For example, the surface slope at the lower flank of Pavonis Mons is steeper than that of around the caldera by about  $4^\circ$ . The uppermost point of the dark feature is

usually located at where the slope turns steeper although the actual altitude varies from mountain to mountain (see Fig. 3 and Table 3). The main part is located on the highly sloped area on the flank of volcanic edifice.

Close-up views of the upper boundary of the coalesced dark streaks reveal that the dark feature is an assemblage of many overlapping spindle-shaped dark streaks (Fig. 1(B) right and Fig. 4), which we term spire streaks. Spire streaks are recognized on all Tharsis Montes.

Each spire streak is spindle-shaped with a length of 1–10 km and width of several hundred meters at the middle part, although the shape at the end of the lower position is ambiguously recognized due to the overlapping of the streaks (Fig. 5). The boundary is usually sharp and rectilinear in kilometer-scaled images. Spire streaks sometimes pass over topographic obstacles such as craters (Fig. 4). No prominent obstacles appear at the starting point of spire streaks (Fig. 5). The linear reticulate ridges we can see in Fig. 5 are believed to be formed by aeolian saltation (Bridges et al., 2010). There exist several bright crater-related wind streaks on the spire streaks, and the upwind sides of the crater-related streaks corresponds to the sharp points of the spire streaks (Fig. 7(B)). In some regions, we can find spire streaks that have different directions at the same place (Fig. 6).

Fig. 7(A) shows the distribution map of spire streaks at the shield volcano, Pavonis Mons in the Tharsis region. Spire streaks are usually at the upper boundary of the dark feature around the caldera of the volcanoes. Most of them are almost parallel to the direction of the maximum slope. It seems that they radiate out from the summit of the Mons.

#### 4. Time-variation of spire streaks

The images obtained by Viking orbiter camera (Carr et al., 1972), Mars Orbiter Camera (MOC) (Malin et al., 1992), THEMIS (Christensen et al., 2004), CTX (Malin et al., 2007) and HiRISE (McEwen et al., 2007) were investigated to determine the time-variation of the spire streaks at Pavonis Mons. Drastic pattern changes were observed only three times between 1976 (the Viking era) and 2007 (the MRO era).

The first change was observed between 1978 and 1999 on the southwestern side of the summit (Fig. 8(A)). The spire streaks, which were not found in the Viking image taken in 1978 but emerged in the Mars Orbiter Camera (MOC) images taken in 1999. The emerged streaks seem to be very clear, although the optics of Viking are different from that of MOC onboard MGS.

The second change was observed between 2001 and 2003 on the southwestern side of the summit again (Fig. 8(B)). A global dust storm (GDS) occurred in 2001 (Cantor, 2007), which was timed between E05-01238 and E09-00848 in Fig. 8(B). We suppose the 2001 GDS caused major changes in the pattern of the spire streaks. The upper boundary of the coalesced dark streaks at the southwestern side shifted to a lower elevation and changed its shape after the 2001 GDS (indicated with red arrows in Fig. 8(B)). The shift was about 0.5 km vertically and 13.7 km horizontally. We have to be careful about the optical depth of dust and other aerosols over the volcano because atmospheric dust and other aerosols sometimes confuse apparent surface changes. Smith (2004) obtained water ice and aerosol optical depth by retrieving infrared spectra returned by the Thermal Emission Spectrometer (TES) onboard MGS. Images in Fig. 8(B) were taken between Mars Year 25,  $L_s=177.81^\circ$ , June 2001 and Mars Year 26,  $L_s=148.92^\circ$ , March 2003. All images were taken in seasons that have relatively high optical depth of dust (i.e. dusty seasons), therefore the absence of the dark features is not because of the difference of optical depth.

**Table 1**  
Instruments.

| Instrument            | Orbiter      | Visible or infrared | Time span                             |
|-----------------------|--------------|---------------------|---------------------------------------|
| Viking orbiter camera | Viking       | Visible             | 1976 August 12 to 1978 March 22       |
| MOC wide angle        | MGS          | Visible             | 1999 April 8 to 2006 August 7         |
| MOC narrow angle      | MGS          | Visible             | 1999 April 8 to 2003 December 11      |
| THEMIS VIS            | Mars Odyssey | Visible             | 2002 March 31 to 2007 November 8      |
| THEMIS IR             | Mars Odyssey | Infrared            | 2002 March 31 to 2007 December 16     |
| CTX                   | MRO          | Visible             | 2006 December 21 to 2007 September 13 |
| HiRISE                | MRO          | Visible             | 2008 August 17                        |

**Table 2**  
Images investigated for this study.

| Instrument            | Image ID | Date       | Solar longitude | Local time |
|-----------------------|----------|------------|-----------------|------------|
| Viking orbiter camera | 052A14   | 1976.8.12  | 107.100796      | 1.099      |
| Viking orbiter camera | 052A15   | 1976.8.12  | 107.10082       | 0.914      |
| Viking orbiter camera | 090A26   | 1976.9.19  | 124.733574      | 1.579      |
| Viking orbiter camera | 090A27   | 1976.9.19  | 124.733598      | 1.483      |
| Viking orbiter camera | 090A28   | 1976.9.19  | 124.733623      | 1.550      |
| Viking orbiter camera | 204A18   | 1977.1.13  | 185.051414      | 22.91      |
| Viking orbiter camera | 210A33   | 1977.1.19  | 188.592285      | 22.62      |
| Viking orbiter camera | 210A35   | 1977.1.19  | 188.592345      | 22.54      |
| Viking orbiter camera | 643A27   | 1978.3.22  | 63.241401       | 21.66      |
| MOC narrow angle      | M0001181 | 1999.4.8   | 121.38          | 14.44      |
| MOC narrow angle      | M1003342 | 1999.12.28 | 271.99          | 13.75      |
| MOC narrow angle      | M1104316 | 2000.1.31  | 292.95          | 13.41      |
| MOC narrow angle      | E0100852 | 2001.2.13  | 116.78          | 14.40      |
| MOC narrow angle      | E0400621 | 2001.5.12  | 159.91          | 14.61      |
| MOC narrow angle      | E0501237 | 2001.6.13  | 177.81          | 14.68      |
| MOC narrow angle      | E0700481 | 2001.8.9   | 210.92          | 14.62      |
| MOC narrow angle      | R0601487 | 2003.6.24  | 209.3           | 14.81      |
| MOC narrow angle      | R1201211 | 2003.12.11 | 314.15          | 13.46      |
| MOC narrow angle      | S0901691 | 2005.8.16  | 270.19          | 13.95      |
| MOC wide angle        | M0001182 | 1999.4.8   | 121.38          | 14.45      |
| MOC wide angle        | M0200994 | 1999.6.10  | 152.18          | 14.56      |
| MOC wide angle        | M0204644 | 1999.6.29  | 162.42          | 14.64      |
| MOC wide angle        | M0301265 | 1999.7.7   | 166.28          | 14.66      |
| MOC wide angle        | M0304996 | 1999.7.26  | 177             | 14.70      |
| MOC wide angle        | M0807220 | 1999.10.29 | 233.63          | 14.42      |
| MOC wide angle        | M0901219 | 1999.11.5  | 238.17          | 14.35      |
| MOC wide angle        | M0905823 | 1999.11.24 | 250.54          | 14.16      |
| MOC wide angle        | M1000152 | 1999.12.1  | 255.11          | 14.08      |
| MOC wide angle        | M1002559 | 1999.12.21 | 267.46          | 13.85      |
| MOC wide angle        | M1003343 | 1999.12.28 | 271.99          | 13.77      |
| MOC wide angle        | M1103510 | 2000.1.24  | 288.57          | 13.50      |
| MOC wide angle        | M1104317 | 2000.1.31  | 292.95          | 13.43      |
| MOC wide angle        | M1202022 | 2000.2.20  | 304.66          | 13.30      |
| MOC wide angle        | M1301144 | 2000.3.17  | 320.13          | 13.19      |
| MOC wide angle        | M1400402 | 2000.4.6   | 331.02          | 13.17      |
| MOC wide angle        | M1902049 | 2000.9.30  | 56.16           | 14.01      |
| MOC wide angle        | M2000389 | 2000.10.7  | 59.32           | 14.05      |
| MOC wide angle        | E0100387 | 2001.2.6   | 113.46          | 14.40      |
| MOC wide angle        | E0100853 | 2001.2.13  | 116.78          | 14.42      |
| MOC wide angle        | E0200097 | 2001.3.2   | 124.49          | 14.33      |
| MOC wide angle        | E0200741 | 2001.3.9   | 127.91          | 14.44      |
| MOC wide angle        | E0300076 | 2001.4.1   | 139.41          | 14.53      |
| MOC wide angle        | E0300844 | 2001.4.9   | 142.99          | 14.56      |
| MOC wide angle        | E0302163 | 2001.4.25  | 151.33          | 14.59      |
| MOC wide angle        | E0400622 | 2001.5.12  | 159.91          | 14.63      |
| MOC wide angle        | E0501238 | 2001.6.13  | 177.81          | 14.69      |
| MOC wide angle        | E0503453 | 2001.6.30  | 187.15          | 14.70      |
| MOC wide angle        | E0900848 | 2001.10.12 | 250.8           | 14.18      |
| MOC wide angle        | E1002897 | 2001.11.19 | 274.82          | 13.76      |
| MOC wide angle        | E1202132 | 2002.1.19  | 312.12          | 13.28      |
| MOC wide angle        | E1302318 | 2002.2.26  | 333.49          | 13.23      |
| MOC wide angle        | R0300438 | 2003.3.8   | 148.92          | 14.72      |
| MOC wide angle        | R0502133 | 2003.5.27  | 192.16          | 14.88      |
| MOC wide angle        | R0600679 | 2003.6.10  | 200.64          | 14.87      |
| MOC wide angle        | R0601488 | 2003.6.24  | 209.3           | 14.83      |
| MOC wide angle        | R0700061 | 2003.7.1   | 213.69          | 14.81      |
| MOC wide angle        | R0900312 | 2003.9.4   | 254.34          | 14.35      |
| MOC wide angle        | R0903551 | 2003.9.26  | 267.99          | 14.08      |

Table 2 (continued)

| Instrument     | Image ID  | Date       | Solar longitude | Local time |
|----------------|-----------|------------|-----------------|------------|
| MOC wide angle | R1000437  | 2003.10.3  | 272.51          | 14.00      |
| MOC wide angle | R1001721  | 2003.10.10 | 277.01          | 13.92      |
| MOC wide angle | R1201212  | 2003.12.11 | 314.15          | 13.48      |
| MOC wide angle | R1203502  | 2003.12.27 | 323.5           | 13.34      |
| MOC wide angle | R1304205  | 2004.1.27  | 340.35          | 13.48      |
| MOC wide angle | R1400388  | 2004.2.3   | 344.16          | 13.56      |
| MOC wide angle | R1702093  | 2004.5.24  | 37.82           | 15.13      |
| MOC wide angle | S0300035  | 2005.2.1   | 153.36          | 14.85      |
| MOC wide angle | S0703290  | 2005.6.30  | 240.26          | 14.52      |
| MOC wide angle | S0801818  | 2005.7.16  | 250.68          | 14.34      |
| MOC wide angle | S0802608  | 2005.7.24  | 255.25          | 14.24      |
| MOC wide angle | S1200904  | 2005.11.10 | 321.43          | 13.39      |
| MOC wide angle | S1500274  | 2006.2.3   | 6.24            | 13.52      |
| MOC wide angle | S1501040  | 2006.2.10  | 9.75            | 13.61      |
| MOC wide angle | S2100386  | 2006.8.7   | 89.55           | 14.34      |
| THEMIS VIS     | V01302016 | 2002.3.31  | 350.92          | 15.22      |
| THEMIS VIS     | V01639008 | 2002.4.28  | 4.86            | 15.39      |
| THEMIS VIS     | V03474007 | 2002.9.26  | 73.456          | 16.44      |
| THEMIS VIS     | V05384021 | 2003.3.2   | 145.817         | 17.11      |
| THEMIS VIS     | V07245001 | 2003.8.2   | 233.568         | 17.24      |
| THEMIS VIS     | V07968022 | 2003.10.1  | 271.293         | 16.71      |
| THEMIS VIS     | V10851006 | 2004.5.25  | 38.337          | 16.74      |
| THEMIS VIS     | V11475011 | 2004.7.16  | 61.099          | 17.00      |
| THEMIS VIS     | V12074014 | 2004.9.3   | 82.646          | 17.17      |
| THEMIS VIS     | V12673013 | 2004.10.22 | 104.531         | 17.29      |
| THEMIS VIS     | V12698013 | 2004.10.24 | 105.461         | 17.30      |
| THEMIS VIS     | V13610001 | 2005.1.7   | 140.894         | 17.48      |
| THEMIS VIS     | V15457001 | 2005.6.9   | 226.715         | 17.46      |
| THEMIS VIS     | V16081001 | 2005.7.30  | 259.201         | 16.97      |
| THEMIS VIS     | V16368001 | 2005.8.23  | 274.102         | 16.71      |
| THEMIS VIS     | V16679017 | 2005.9.17  | 290.008         | 16.45      |
| THEMIS VIS     | V16991018 | 2005.10.13 | 305.449         | 16.27      |
| THEMIS VIS     | V17278013 | 2005.11.6  | 319.148         | 16.18      |
| THEMIS VIS     | V25265011 | 2007.8.25  | 302.043         | 16.48      |
| THEMIS VIS     | V26176016 | 2007.11.8  | 344.108         | 16.40      |
| THEMIS IR      | I01302015 | 2002.3.31  | 350.92          | 15.22      |
| THEMIS IR      | I01639007 | 2002.4.28  | 4.86            | 15.40      |
| THEMIS IR      | I01808002 | 2002.5.12  | 11.609          | 3.473      |
| THEMIS IR      | I01833002 | 2002.5.14  | 12.599          | 3.498      |
| THEMIS IR      | I01858006 | 2002.5.16  | 13.585          | 3.520      |
| THEMIS IR      | I02001008 | 2002.5.28  | 19.197          | 15.62      |
| THEMIS IR      | I02195002 | 2002.6.13  | 26.632          | 3.735      |
| THEMIS IR      | I03474006 | 2002.9.26  | 73.456          | 16.44      |
| THEMIS IR      | I03500001 | 2002.9.28  | 74.355          | 16.46      |
| THEMIS IR      | I05216002 | 2003.2.16  | 138.886         | 5.047      |
| THEMIS IR      | I05553005 | 2003.3.16  | 152.906         | 5.167      |
| THEMIS IR      | I05578022 | 2003.3.18  | 153.972         | 5.173      |
| THEMIS IR      | I06327024 | 2003.5.19  | 187.728         | 5.383      |
| THEMIS IR      | I06857011 | 2003.7.2   | 213.741         | 17.36      |
| THEMIS IR      | I06882014 | 2003.7.4   | 215.004         | 17.36      |
| THEMIS IR      | I07051011 | 2003.7.18  | 223.585         | 5.348      |
| THEMIS IR      | I07219010 | 2003.7.31  | 232.274         | 17.22      |
| THEMIS IR      | I07388022 | 2003.8.14  | 241.031         | 5.157      |
| THEMIS IR      | I07413016 | 2003.8.16  | 242.335         | 5.139      |
| THEMIS IR      | I07438011 | 2003.8.18  | 243.637         | 5.182      |
| THEMIS IR      | I07750016 | 2003.9.13  | 259.936         | 4.942      |
| THEMIS IR      | I07775015 | 2003.9.15  | 261.241         | 4.901      |
| THEMIS IR      | I07800012 | 2003.9.17  | 262.544         | 4.873      |
| THEMIS IR      | I07968021 | 2003.10.1  | 271.292         | 16.78      |
| THEMIS IR      | I08112012 | 2003.10.13 | 278.682         | 4.575      |
| THEMIS IR      | I11787007 | 2004.8.10  | 72.318          | 17.11      |
| THEMIS IR      | I13753002 | 2005.1.19  | 146.825         | 5.501      |
| THEMIS IR      | I13778009 | 2005.1.21  | 147.87          | 5.505      |
| THEMIS IR      | I14377006 | 2005.3.12  | 174.032         | 5.619      |
| THEMIS IR      | I15575007 | 2005.6.18  | 232.837         | 5.373      |
| THEMIS IR      | I16679016 | 2005.9.17  | 290.008         | 16.46      |
| THEMIS IR      | I16848012 | 2005.10.1  | 298.412         | 4.360      |
| THEMIS IR      | I17110010 | 2005.10.23 | 311.167         | 4.226      |
| THEMIS IR      | I17135007 | 2005.10.25 | 312.362         | 4.216      |
| THEMIS IR      | I17160010 | 2005.10.27 | 313.555         | 4.157      |
| THEMIS IR      | I17278012 | 2005.11.6  | 319.148         | 16.17      |
| THEMIS IR      | I17422009 | 2005.11.17 | 325.802         | 4.129      |
| THEMIS IR      | I17447013 | 2005.11.19 | 326.946         | 4.154      |
| THEMIS IR      | I17615023 | 2005.12.3  | 334.562         | 16.15      |
| THEMIS IR      | I18214015 | 2006.1.22  | 0.209           | 16.35      |

Table 2 (continued)

| Instrument | Image ID                   | Date       | Solar longitude | Local time |
|------------|----------------------------|------------|-----------------|------------|
| THEMIS IR  | I18526008                  | 2006.2.16  | 12.779          | 16.48      |
| THEMIS IR  | I18982003                  | 2006.3.26  | 30.357          | 4.685      |
| THEMIS IR  | I19437014                  | 2006.5.2   | 47.256          | 16.96      |
| THEMIS IR  | I19631001                  | 2006.5.18  | 54.3            | 4.993      |
| THEMIS IR  | I21765022                  | 2006.11.10 | 133.286         | 5.553      |
| THEMIS IR  | I23443003                  | 2007.3.28  | 208.625         | 17.75      |
| THEMIS IR  | I23730021                  | 2007.4.21  | 223.154         | 17.65      |
| THEMIS IR  | I24017011                  | 2007.5.14  | 237.983         | 17.48      |
| THEMIS IR  | I24042015                  | 2007.5.16  | 239.284         | 17.46      |
| THEMIS IR  | I24329008                  | 2007.6.9   | 254.267         | 17.22      |
| THEMIS IR  | I24354011                  | 2007.6.11  | 255.573         | 17.20      |
| THEMIS IR  | I24473008                  | 2007.6.21  | 261.756         | 5.063      |
| THEMIS IR  | I24641012                  | 2007.7.5   | 270.509         | 16.92      |
| THEMIS IR  | I24666012                  | 2007.7.7   | 271.801         | 16.91      |
| THEMIS IR  | I24978011                  | 2007.8.2   | 287.756         | 16.65      |
| THEMIS IR  | I25265010                  | 2007.8.25  | 302.044         | 16.46      |
| THEMIS IR  | I26607013                  | 2007.12.14 | 2.2             | 4.581      |
| THEMIS IR  | I26632017                  | 2007.12.16 | 3.219           | 4.597      |
| CTX        | P02_001893_1804_XN_00N113W | 2006.12.21 | 154.13          | 15.61      |
| CTX        | P03_002249_1803_XL_00N112W | 2007.1.8   | 168.88          | 15.68      |
| CTX        | P04_002671_1792_XL_00S113W | 2007.2.20  | 187.3           | 15.73      |
| CTX        | P07_003805_1805_XN_00N112W | 2007.5.19  | 241.2           | 15.32      |
| CTX        | P08_004016_1805_XL_00N113W | 2007.6.5   | 251.62          | 15.18      |
| CTX        | P08_004227_1826_XL_02N113W | 2007.6.21  | 262.05          | 14.99      |
| CTX        | P09_004517_1805_XL_00N113W | 2007.7.14  | 276.27          | 14.59      |
| CTX        | P09_004728_1805_XL_00N112W | 2007.7.30  | 286.46          | 14.49      |
| CTX        | P10_004794_1813_XL_01N112W | 2007.8.5   | 289.61          | 14.57      |
| CTX        | P10_004939_1809_XL_00N112W | 2007.8.16  | 296.47          | 14.39      |
| CTX        | P10_005005_1806_XL_00N112W | 2007.8.21  | 299.56          | 14.48      |
| CTX        | P11_005150_1808_XL_00N112W | 2007.9.1   | 306.27          | 14.33      |
| CTX        | P11_005295_1822_XL_02N113W | 2007.9.13  | 312.87          | 14.19      |
| HIRISE     | PSP_009646_1795            | 2008.8.17  | 113.8           | 15.48      |

THEMIS VIS onboard Mars Odyssey also observed the variation (Fig. 1(B)). The spire streaks once erased by GDS 2001 later re-formed, although the exact timescale of the formation cannot be specified because of the limited number of images during this period.

The third change was observed between 2004 and 2005 also on the southwestern side of the summit (Fig. 8(C)). Linear streaks that were not found in R14-00388 appeared in S08-02608.

In summary, we observed large changes in the morphology of the spire streaks only a few times between 1976 and 2007, although we should note that we do not know overall rate of the formation of the spire streaks because there could have been streaks formed during the times when image coverage was lacking. We conclude that GDS and local dust storms might be responsible for erasing the spire streaks, and the formation of the spire streaks is not a frequent occurrence.

## 5. Interpretation and implications for spire streak formation

Crater-related wind streaks at the coalesced dark streaks indicate that the spindle-shaped side of the spire streaks at higher altitude is the up-stream direction of the wind. Wind patterns in Fig. 7(A) organize in the downslope direction all around the volcano and within the caldera. Those are in agreement with atmospheric circulations dominated by nighttime katabatic acceleration. In nighttime conditions over Martian and terrestrial topographical slopes, radiative cooling occur at the surface and temperature inversions take place in the near-surface atmosphere, which leads to katabatic circulations while cooled dense air is accelerated down sloping terrains by gravity (see review by Spiga, *in press*, and references therein). Large near-surface

inversions yield Martian katabatic winds two to three times larger than on Earth despite the much lower gravity on the Red Planet. Katabatic winds on Mars can reach extreme values of 40–50 m s<sup>-1</sup> (those maximum values are usually found a few hundreds meters above the surface).

This interpretation is supported through comparisons between maps of wind direction derived from spire streaks analysis (Fig. 7) and near-surface predictions from mesoscale modeling (Fig. 9 at local time 10:00 pm). Best agreement between both wind fields is obtained during the night from local times 08:00 pm to 05:00 am. Fig. 10 shows that upslope anabatic winds are prominent in the daytime wind regime which indicates those as well would be able to lift material from the surface. However, daytime wind regime appears a less consistent scenario than its nighttime katabatic counterpart: neither the downslope orientation of spire streaks nor their radial distribution (notably in the Pavonis caldera) are accounted for. Furthermore, Fig. 10 shows that daytime wind regime undergoes significant temporal variability in the area of interest, while nighttime wind regime is similar to Fig. 9 all night long, hence more prone to impact distribution of surface material. The preferential formation of geological structures aligned with winds during nighttime was already noticed in previous studies (Greeley and Thompson, 2003). Correlations between modeled and observed wind directions indicate that nighttime stable conditions might be key to form spire streaks, which could be used as an indirect evidence for intense katabatic winds over Pavonis and, more generally, Tharsis volcanoes. Note that we only present simulations at a given season, but strong nighttime katabatic circulations persist throughout the year (with similar amplitudes) over the Tharsis volcanoes.

Magalhaes and Gierasch (1982) used an analytic one-dimensional model to determine friction velocities over Martian slopes. Their results are suggestive of active downslope aeolian

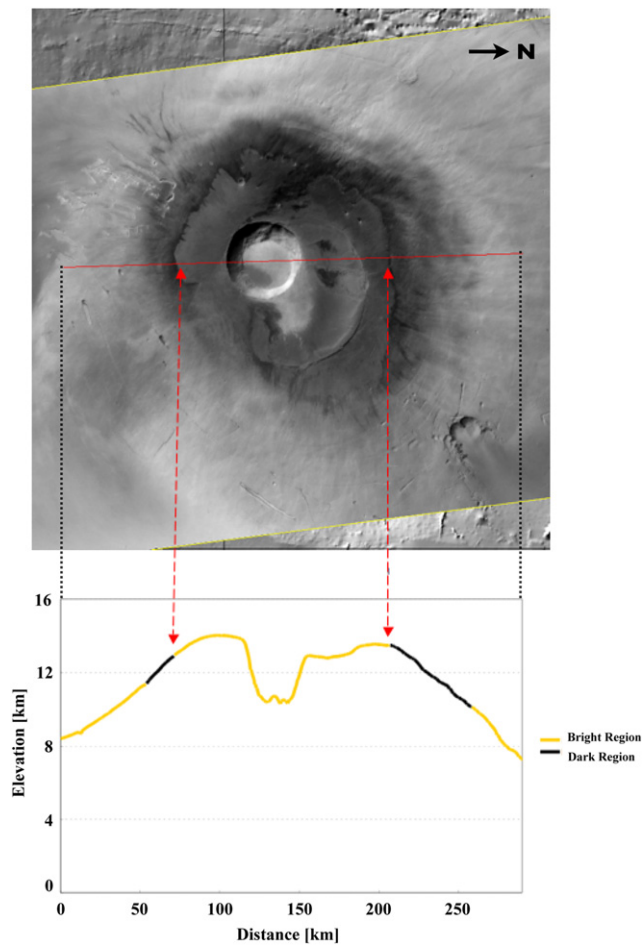


**Fig. 3.** Topography of Pavonis Mons. Mission Experiment Gridded Data Records (MEGDRs) of Mars Orbiter Laser Altimeter (MOLA) are used to derive this figure. The spatial resolution of the MEGDRs is about 0.46 km/pixel. Black and yellow lines indicate dark and bright surface region respectively. There are many spire streaks at the upper boundary of the dark region. (For interpretation of the references to color in this figure legend, the reader is referred to the web version of this article.)

**Table 3**  
Height and flank slopes at coalesced dark streaks.

| Volcano                                    | Olympus | Ascræus | Pavonis | Arsia |
|--|---------|---------|---------|-------|
| Height of upper limit of dark streaks (km) | 15–21   | 15–18   | 12–14   | 16–18 |
| Height of lower limit of dark streaks (km) | 9–15    | 9–14    | 9–12    | 12–17 |
| Flank slope (by Plescia, 2004) (deg)       | 5.2     | 7.4     | 4.3     | 5.1   |

transport at nighttime on slopes favored by coalesced dark streaks. Three-dimensional mesoscale simulations described in this paper agree with these earlier estimates: maximum values for friction velocities reach  $1.5 \text{ m s}^{-1}$ , which can move particles whose grain size of around  $100 \mu\text{m}$  (Shao and Lu, 2000). In addition, predictions of friction velocity around the caldera and main slope showed that streaks are observed just at locations where most of higher values of friction velocity concentrate in the mesoscale simulations.

While kilometer-scale simulations do capture the mesoscale wind directions indicated by streaks (for a typical year devoid of planet-circling dust storms), sub-kilometer scale images such

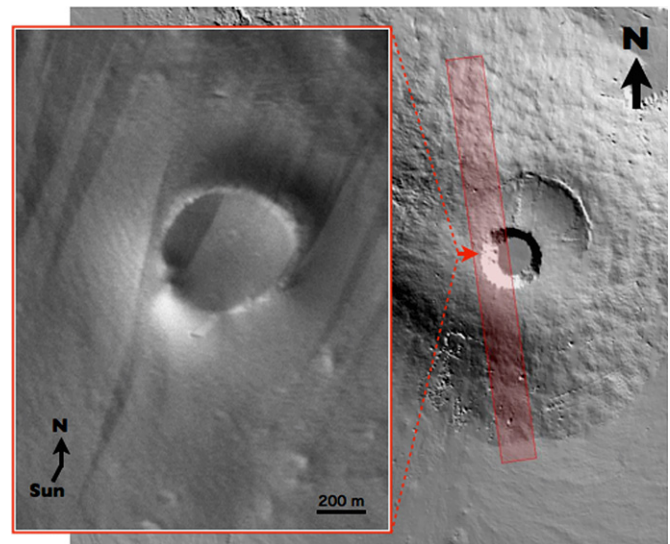


**Fig. 4.** (Left) A spire streak that passed over an impact crater. The southwest side of the crater is bright because of sun illumination. (Right) The place of CTX image P08\_004016\_1805\_XL\_00N113W as a red square is shown on MOLA shaded relief of Pavonis Mons generated by JMARS (see <http://jmars.asu.edu/> for additional information about JMARS). The spire streak is at  $0.61^\circ\text{N}$ ,  $246.69^\circ\text{E}$ . (For interpretation of the references to color in this figure legend, the reader is referred to the web version of this article.)

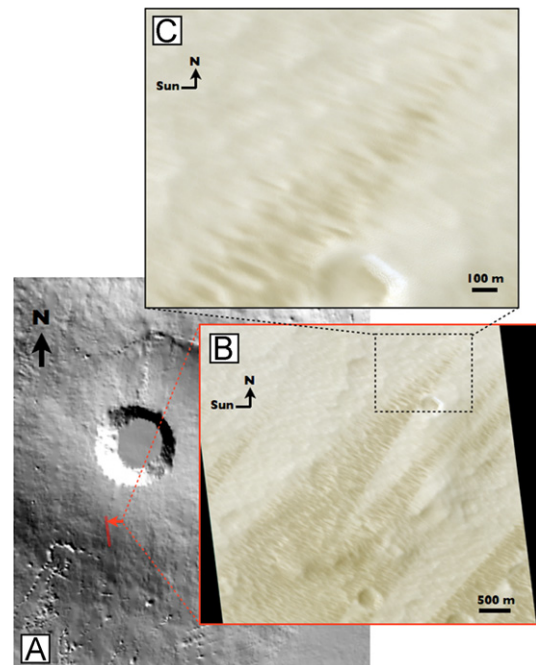


**Fig. 5.** (A) The place of HiRISE image PSP\_009646\_1795\_COLOR as a red square is shown on MOLA shaded relief of Pavonis Mons generated by JMARS (see <http://jmars.asu.edu/> for additional information about JMARS). (B) An example of a spire streak. Each spire streak is spindle-shaped with length of 1–10 km and width of several hundred meters at the middle part, although the shape at the end of the lower position is ambiguous due to the overlappings. (C) A close-up image of the start point of a spire streak. There seem to be no prominent obstacles at the start point of the many spire streaks. The linear reticulate ridges both inside and outside the streaks are believed to be formed by aeolian saltation (Bridges et al., 2010). Winds may have saltated denser particle and formed the linear reticulate ridges. The removal of the finer dust-sized material from the surface by winds might have caused the dark albedo of the streaks. (For interpretation of the references to color in this figure legend, the reader is referred to the web version of this article.)

as Fig. 6 reveal overlapping structures pointing out different wind directions. Each spire streak indicates maximum wind events, possibly reflecting exceptional meteorological conditions. Thus,

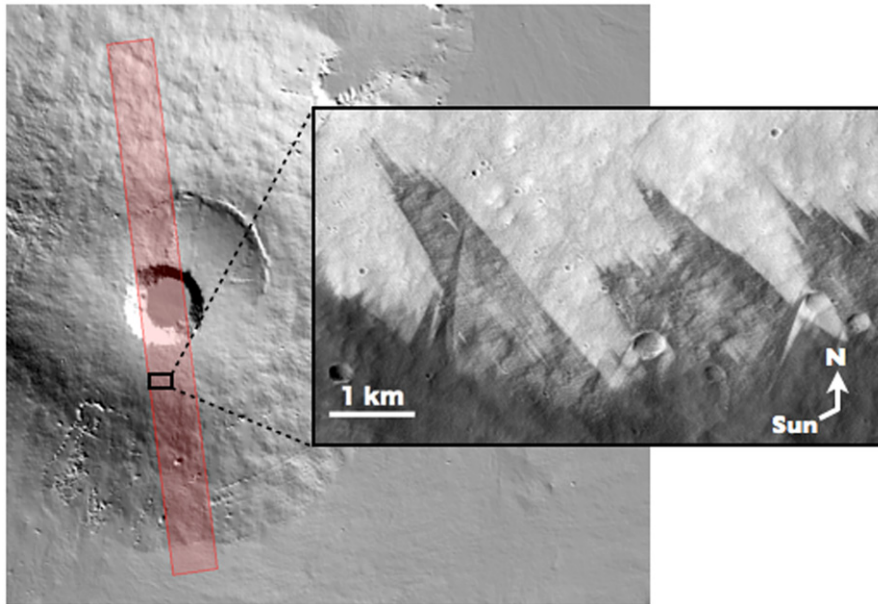


**Fig. 6.** (Left) The place of CTX image P07\_003805\_1805\_XN\_00N112W as a red square is shown on MOLA shaded relief of Pavonis Mons generated by JMARS (see <http://jmars.asu.edu/> for additional information about JMARS). (Right) Spire streaks at the southern flank of Pavonis Mons. The spire streaks which have different directions overlap at the same place (0.41°S, 247.07°E). (For interpretation of the references to color in this figure legend, the reader is referred to the web version of this article.)

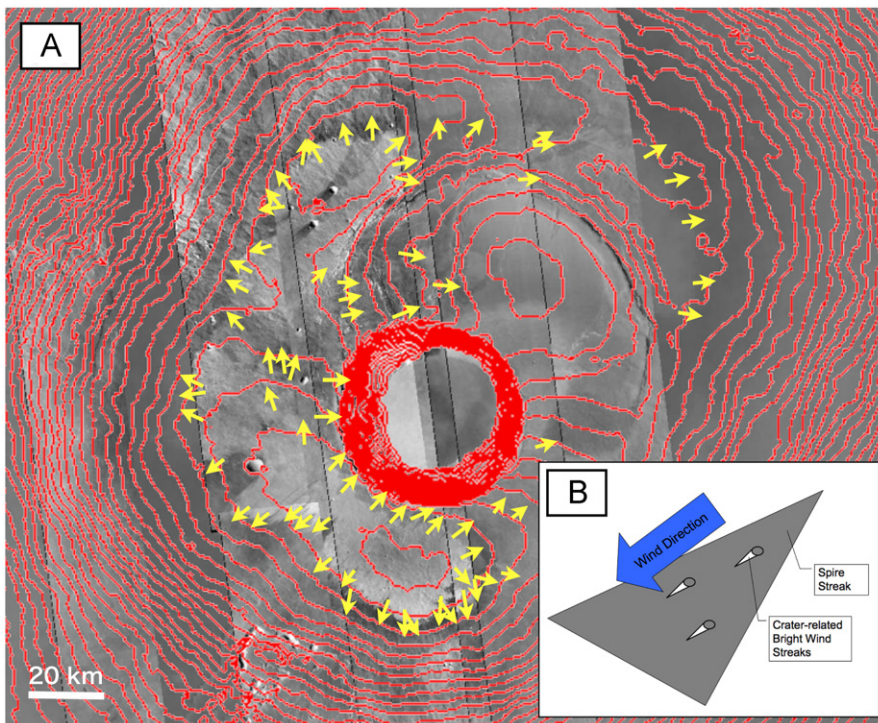


**Fig. 7.** (A) A distribution map of the spire streaks at Pavonis Mons. Contour lines (by 200 m) are shown on a mosaic image of CTX (generated by JMARS: <http://jmars.asu.edu/>). Yellow arrows indicate spire streaks, and the roots of the arrows show the inferred upwind direction. The number of arrows does not reflect the exact number of the spire streaks, because there are so many spire streaks. (B) Schematic diagram explaining how we estimate the wind direction. Crater-related bright wind streaks on the spire streaks indicate that the narrow side of the spire streak is the upstream side of the wind. (For interpretation of the references to color in this figure legend, the reader is referred to the web version of this article.)

structures not oriented towards the average katabatic direction could be caused e.g. by dust storms which both reinforce large-scale winds and lower local katabatic winds. Dust storms (and the subsequent irregular interannual variability of the Martian climate) might explain why drastic changes in the shape of the

spire streaks at the southwestern side of the caldera of Pavonis Mons are observed between 1999 and 2007 (where two planet-encircling dust storms occurred), while almost no changes are noted between March 2003 and February 2004 (where the annual dust cycle follows a “non-dusty year” trend).

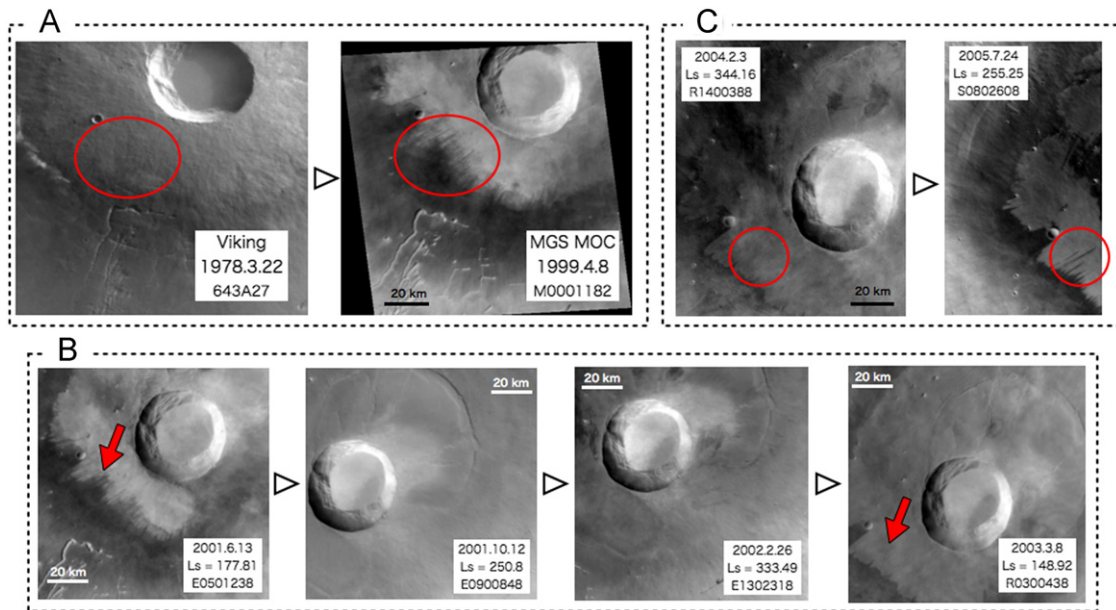


**Fig. 8.** (A) Temporal changes of the spire streaks from 1978 to 1999. The left image was taken by Viking orbiter (incidence angle =  $81.60^\circ$ , phase angle =  $96.75^\circ$ ), and the right image was taken by MOC MGS (incidence angle =  $42.04^\circ$ , phase angle =  $39.21^\circ$ ). (B) Temporal changes of the spire streaks from May 2001 to May 2003. All images are taken by MGS MOC. The perihelion season ( $L_s = 180^\circ$ – $360^\circ$ ) is relatively dusty (Smith, 2004). E09-00848 was taken at highly dusty moment after the global dust storm of 2001, while the other images were taken under slightly lower optical depth than E09-00848. The (incidence angle, phase angle) of the images are ( $40.59^\circ$ ,  $37.16^\circ$ ), ( $39.99^\circ$ ,  $50.16^\circ$ ), ( $21.58^\circ$ ,  $31.97^\circ$ ), and ( $42.43^\circ$ ,  $35.47^\circ$ ) starting from the left. (C) Temporal changes of the spire streaks from February 2004 to July 2005. All images were taken by MOC MGS. The (incidence angle, phase angle) of the images are ( $25.02^\circ$ ,  $26.34^\circ$ ) and ( $41.09^\circ$ ,  $5573^\circ$ ) starting from the left. (For interpretation of the references to color in this figure legend, the reader is referred to the web version of this article.)

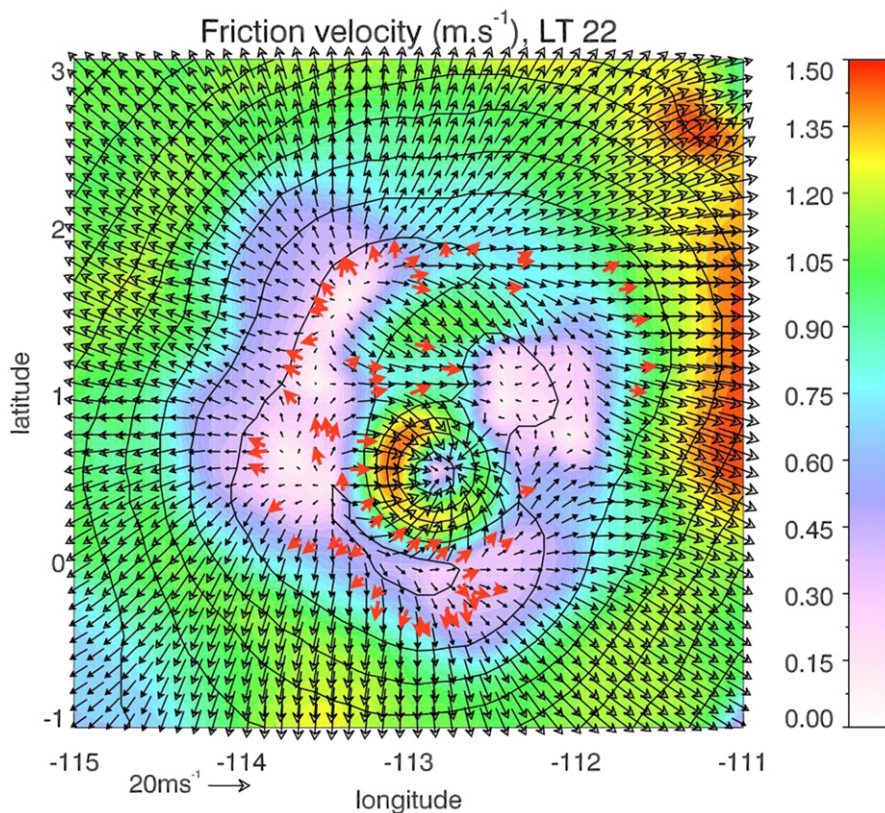


**Fig. 9.** Values of friction velocity predicted by the Spiga and Forget (2009) mesoscale model over Pavonis Mons at local time 10:00 pm. Wind vectors 3 m above the local surface are superimposed and showed with black arrows. Contours represent the MOLA topography interpolated to the model's horizontal grid. Red arrows indicate spire streaks, and the roots of the arrows show the inferred upwind direction (same as Fig. 7(A)). Friction velocity is calculated from wind predicted in the first vertical model level (located 3 m above the surface) under the usual "logarithmic surface layer" assumption (see Section 2.2). (For interpretation of the references to color in this figure legend, the reader is referred to the web version of this article.)

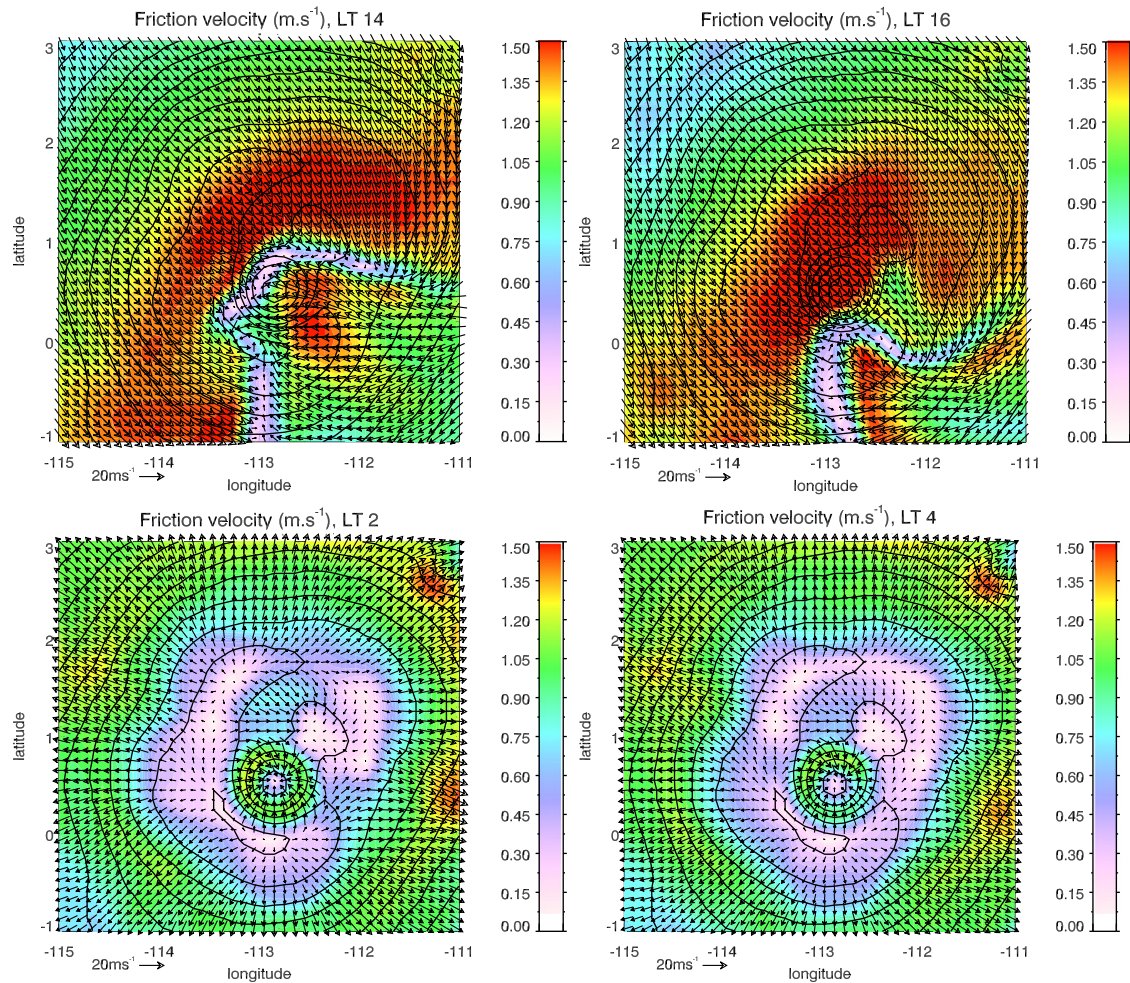


**Fig. 10.** Same as Fig. 9, but for local times 02:00 pm and 04:00 pm (top) and 02:00 am and 04:00 am (bottom) in order to illustrate wind variability with local time.

The spire streaks have been thought of an erosional origin. The dark features on Mars are conventionally attributed to relatively dust-free but still dominantly particulate materials ranging from 0.1 mm to 1 cm rather than bedrock (Christensen and Moore, 1992). The bright region around the spire streaks has high value of the Dust Cover Index (DCI) derived by Ruff and Christensen (2002), and the coalesced dark streaks have relatively low value of the DCI. This suggests that removal of fine-grained dust at the spire streaks causes the dark albedo feature. However, we cannot specify the size of removed particles which is responsible for the dark albedo because the value of the friction velocities which we obtained (from 0.5 to 1.5  $\text{m s}^{-1}$ ) do not show the exact friction velocity under which the spire streaks were formed. Dark wind streaks are classified into two categories (Thomas et al., 1981). (1) Depositional dark streaks, which are interpreted to be formed by deposition of dark material moved by saltation. (2) Erosional dark streaks, which display the surface as formed by aeolian erosion.

Depositional darks wind streaks need local sources or topographic traps for dark material (Geissler et al., 2008). The spire streaks do not belong to this category because there seems no apparent source material at the origin (Fig. 5). Thermal inertia, which is defined by thermal conductivity, bulk density and specific heat capacity, is used as an important parameter to characterize the surface materials by remote sensing (Putzig et al., 2005; Mellon et al., 2000). The quantitative comparison of thermal inertia by Putzig et al. (2005) does not show a significant

difference between the dark albedo region where spire streaks exist and its surroundings; both have low value of thermal inertia ( $30\text{--}200 \text{ J m}^{-2} \text{ K}^{-1} \text{ s}^{-1/2}$ ). Thus, the difference in albedo should be confined to a surface layer less than the thickness of the skin depth at the period of a day (several cm), which is the principal timescale for the determination of thermal inertia. The spire streaks could belong to category (2) in which high winds sweep away fine particulate material.

The removal of fine particulate material can account for the spire streaks being darker than the surroundings. The linear reticulate ridges both inside and outside the streaks are believed to be formed by aeolian saltation (Bridges et al., 2010). Winds may have saltated denser particle and formed the linear reticulate ridges. The removal of the finer dust-sized material from the surface by winds might have caused the dark albedo of the streaks, although we cannot identify the sequential order of the formation of the reticulate ridges and the formation of the dark albedo feature. In this case, winds cannot make any difference in the thermal inertia of the units because winds only can affect a much thinner layer of the surface materials than the thermal skin depth associated with the daily variation of the insolation. The existence of bright crater-related wind streaks on the dark spire streaks (Fig. 6) indicates the erosional processes; the rim of crater prevented winds from removing fine particulate materials and preserved the bright surface on the leeward side of the crater. The dark albedo of them seems to be consistent with the erosional origin so far.

However, some features of the spire streaks reported in this paper are outside the scope of previous modeling for the erosional origin. If the spire streaks are erosional streaks, atmospheric turbulence to cause erosion has to originate at point-like source at first, then it will grow wider as blowing down the slope. Detailed modeling of formation of spindle-shaped erosional streaks such as the spire streaks is still lacking, although the basic modeling for erosional streaks without topographic obstacles already exists (Magalhaes and Gierasch, 1982). The morphology exhibiting straight pass over topographic obstacles (Fig. 4) could not be explained by the ordinary model for erosional processes. We need a new erosional model for the formation of the spire streaks to account for the spindle-shape and passing over topographic obstacles.

## 6. Conclusions

We documented the distribution and time-variation of the spire streaks. Recent high-resolution images enabled us to document the streaks under more specific conditions than ever. Our investigation showed that the spire streaks are erosional features which are outside the scope of previous modeling for erosional process. Strong katabatic winds at nighttime, which travel down Pavonis Mons, caused the formation of the spire streaks. A spire streak looks darker than its surroundings because the wind removed the finer dust-sized material from the surface. Each spire streak indicates maximum wind events, possibly reflecting exceptional meteorological conditions, although katabatic winds close to topographical obstacles during Martian nights are powerful each and every night all year long. Dust storms (and other possible irregular variability of the Martian climate) might explain the time variation of the spire streaks. Detailed modeling of the formation of the spire streaks is needed to explain the morphology of the spire streaks with erosional processes.

## Acknowledgments

This work was supported by the grant-in-aid for JSPS Fellows. We wish to thank Dr. Paul Geissler and the anonymous reviewer for constructive and helpful reviews of this manuscript. We would like to thank Viking orbiter camera, MOLA, MOC, THEMIS, HiRISE, and CTX engineering and scientific teams for making this work possible.

## References

- Bridges, N.T., Banks, M.E., Beyer, R.A., Chuang, F.C., Noe Doobrea, E.Z., Herkenhoff, K.E., Keszthelyi, L.P., Fishbaugh, K.E., McEwen, A.S., Michaels, T.I., Thomson, B.J., Wray, J.J., 2010. Aeolian bedforms, yardangs, and indurated surfaces in the Tharsis Montes as seen by the HiRISE camera: evidence for dust aggregates. *Icarus* 205, 165–182. doi:10.1016/j.icarus.2009.05.017.
- Cantor, B., 2007. MOC observations of the 2001 Mars planet-encircling dust storm. *Icarus* 186, 60–96. doi:10.1016/j.icarus.2006.08.019.
- Carr, M.H., Baum, W.A., Briggs, G.A., Masursky, H., Wise, D.W., Montgomery, D.R., 1972. Imaging experiment: the viking Mars orbiter. *Icarus* 16, 17–33.
- Christensen, P.R., Moore, H.J., 1992. The martian surface layer. In: *Mars*. University Arizona Press, pp. 686–729.
- Christensen, P.R., Jakosky, B.M., Kieffer, H.H., Malin, M.C., Madsen Jr., H.Y., Nealon, K., Mehall, G.L., Silverman, S.H., Ferry, S., Caplinger, M., Ravine, M., 2004. The thermal emission imaging system (THEMIS) for the Mars 2001 odyssey mission. *Space Science Reviews* 110, 85–130.
- Chuang, F.C., Beyer, R.A., McEwen, A.S., Thomson, B.J., 2007. HiRISE observations of slope streaks on Mars. *Geophysical Research Letters* 34, L20204. doi:10.1029/2007GL031111.
- Chuang, F.C., Beyer, R.A., Bridges, N.T., 2010. Modification of martian slope streaks by eolian processes. *Icarus* 205, 154–164. doi:10.1016/j.icarus.2009.07.035.
- Fischer, E.M., Pieters, C.M., 1993. The continuum slope of Mars: bidirectional reflectance investigations and implications to Olympus Mons. *Icarus* 102, 185–202.
- Geissler, P.E., 2005. Three decades of Martian surface changes. *Journal of Geophysical Research* 110, E02001. doi:10.1029/2004JE002345.
- Geissler, P.E., Johnson, J.R., Sullivan, R., Herkenhoff, K., Mittlefehldt, D., Ferguson, R., Ming, D., Morris, R., Squyres, S., Soderblom, L., Golombek, M., 2008. First in situ investigation of a dark wind streak on Mars. *Journal of Geophysical Research* 113, E12531. doi:10.1029/2008JE003102.
- Greeley, R., Kuzmin, R.O., Rafkin, S.C.R., Michaels, T.I., Haberle, R., 2003. Wind-related features in Gusev crater, Mars. *Journal of Geophysical Research* 108, E12,8077. doi:10.1029/2002JE002006.
- Greeley, R., Thompson, S.D., 2003. Mars: Aeolian features and wind predictions at the Terra Meridiani and Isidis Planitia potential Mars Exploration Rover landing sites. *Journal of Geophysical Research* 108, E128093. doi:10.1029/2003JE002110.
- Lee, S.W., Thomas, P.C., Veverka, J., 1982. Wind streaks in Tharsis and Elysium—implications for sediment transport by slope winds. *Journal of Geophysical Research* 87, 10025–10041.
- Magalhaes, J., Gierasch, G., 1982. A model of martian slope winds: implications for eolian transport. *Journal of Geophysical Research* 87 (B12), 9975–9984.
- Malin, M.C., Danielson, G.E., Ingersoll, A.P., Masursky, H., Veverka, J., Ravine, M.A., Soulanille, T.A., 1992. Mars observer camera. *Journal of Geophysical Research* 97 (E5), 7699–7718.
- Malin, M.C., Bell III, J.F., Cantor, B.A., Caplinger, M.A., Calvin, W.M., Clancy, R.T., Edgett, K.S., Edwards, L., Haberle, R.M., James, P.B., Lee, S.W., Ravine, M.A., Thomas, P.C., Wolff, M.J., 2007. Context camera investigation on board the Mars reconnaissance orbiter. *Journal of Geophysical Research* 112, E5504. doi:10.1029/2006JE002808.
- McEwen, A.S., Eliason, E.M., Bergstrom, J.W., Bridges, N.T., Hansen, C.J., Delamere, W.A., Grant, J.A., Gulick, V.C., Herkenhoff, K.E., Keszthelyi, L., Kirk, R.L., Mellon, M.T., Squyres, S.W., Thomas, N., Weitz, C.M., 2007. Mars reconnaissance orbiter's high resolution imaging science experiment (HiRISE). *Journal of Geophysical Research* 112, E5S02. doi:10.1029/2005JE002605.
- Mellon, M.T., Jakosky, B.M., Kieffer, H.H., Christensen, P.R., 2000. High-resolution thermal inertia mapping from the Mars global surveyor thermal emission spectrometer. *Icarus* 148, 437–455.
- Newman, C.E., Lewis, S.R., Read, P.L., Forget, F., 2002. Modeling the Martian dust cycle. 1. Representations of dust transport processes. *Journal of Geophysical Research* 107, E125123. doi:10.1029/2002JE001910.
- Plescia, J.B., 2004. Morphometric properties of Martian volcanoes. *Journal of Geophysical Research* 109, E03003. doi:10.1029/2002JE002031.
- Putzig, N.E., Mellon, M.T., Kretke, K.A., Arvidson, R.E., 2005. Global thermal inertia and surface properties of Mars from the MGS mapping mission. *Icarus* 173, 325–341. doi:10.1016/j.icarus.2004.08.017.
- Ruff, S.W., Christensen, P.R., 2002. Bright and dark regions on Mars: particle size and mineralogical characteristics based on Thermal Emission Spectrometer data. *Journal of Geophysical Research* 107, E125127. doi:10.1029/2001JE001580.
- Sagan, C., Veverka, J., Steinbacher, R., Quam, L., Tucker, R., Eross, B., 1974. Variable features on Mars. IV. Pavonis Mons. *Icarus* 22, 24–47.
- Shao, Y., Lu, H., 2000. A simple expression for wind erosion threshold friction velocity. *Journal of Geophysical Research* 105 (D17), 22437–22443.
- Singer, R.B., Roush, T.L., 1983. Spectral reflectance properties of particulate weathered coatings on rocks: laboratory modeling and applicability to Mars. In: *Lunar and Planetary Science Conference XIV*, pp. 708–709.
- Smith, M.D., 2004. Interannual variability in TES atmospheric observations of Mars during 1999–2003. *Icarus* 167, 148–165. doi:10.1016/j.icarus.2003.09.010.
- Smith, M.D., 2009. THEMIS observations of Mars aerosol optical depth from 2002–2008. *Icarus* 202, 444–452. doi:10.1016/j.icarus.2009.03.027.
- Spiga, A., Elements of comparison between Martian and terrestrial mesoscale meteorological phenomena: Katabatic winds and boundary layer convection. *Planetary and Space Science*, in press. doi:10.1016/j.pss.2010.04.025.
- Spiga, A., Forget, F., 2009. A new model to simulate the Martian mesoscale and microscale atmospheric circulation: validation and first results. *Journal of Geophysical Research* 114, E02009. doi:10.1029/2008JE003242.
- Spiga, A., Lewis, S.R., 2010. Martian mesoscale and microscale wind variability of relevance for dust lifting. *Mars* 5, 146–158. doi:10.1555/mars.2010.0006.
- Sullivan, R.S., Thomas, P., Veverka, J., Malin, M., Edgett, K.S., 2001. Mass movement slope streaks imaged by the Mars Orbiter Camera. *Journal of Geophysical Research* 106 (E10), 23607–23633.
- Thomas, P., Veverka, J., Gineris, D., Wong, L., 1984. "Dust" streaks on Mars. *Icarus* 60, 161–179.
- Thomas, P., Veverka, J., Lee, S., Bloom, A., 1981. Classification of wind streaks on Mars. *Icarus* 45, 124–153.
- Wells, E.N., Veverka, J., Thomas, P., 1984. Mars: experimental study of albedo changes caused by dust fallout. *Icarus* 58, 331–338.
- Zuber, M.T., Smith, D.E., Solomon, S.C., Muhleman, D.O., Head, J.W., Garvin, J.B., Abshire, J.B., Bufton, J.L., 1992. The Mars Observer Laser Altimeter Investigation. *Journal of Geophysical Research* 97 (E5), 7781–7797.